AIAA JOURNAL
Vol. 34, No. 8, August 1996

Structure of Coherent Instabilities in a Supersonic Shear Layer

Steven Martens,* Kevin W. Kinzie†, and Dennis K. McLaughlin‡
Pennsylvania State University, University Park, Pennsylvania 16802

Detailed measurements have been made of the instabilities present in supersonic shear layers. A high-speed stream of Mach number 3 or 4 and a low-speed stream of Mach number 1.2 are produced and begin mixing at the trailing edge of the dividing centerbody. Glow discharge excitation is used to excite either two-dimensional or oblique instability waves. Mach-number profiles for the Mach 3 case show little effect of excitation on the growth rate, whereas the higher Mach number case shows enhanced mixing with both excitation geometries. Four hot wires are used simultaneously to measure the axial and spanwise wavelengths for each case. With these wavelengths, the propagation angles of the instabilities are calculated. The instability waves in a two-dimensionally excited shear layer remain two dimensional. The three-dimensionally excited shear layer results in waves that travel at a nominal angle of approximately 60 deg to the mean flow direction, even with three widely different excitation angles. Increasing the convective Mach number of the shear layer results in a slightly larger oblique instability wave angle. The conclusions support the predictions of analytical and/or numerical studies.

Nomenclature

a	= speed of sound
f	= frequency
f_c	= characteristic frequency, U_1/δ_ω
f_e	= excitation frequency
M	= Mach number
M_c	= convective Mach number
P_{01}	= total pressure in the high-speed stream
Re	= unit Reynolds number based on the properties in the high-speed stream
St	= Strouhal number, f/f_c
U	= time mean velocity
β	= propagation angle of instability waves
β_e	= angle of excitation
δ_ω	= local vorticity thickness
λ	= wavelength

Subscripts

1	= high-speed stream
2	= low-speed stream

Introduction

WITH the resurgence of interest in hypersonic aerodynamics, there is an acknowledged need for a more fundamental understanding of compressible-shear-layer mixing. This need is especially prevalent in the development of scramjet engines. Fuel is injected into a supersonic stream of air and then burned. It has long been documented that as the speed differential between two parallel gas streams approaches and exceeds supersonic values, the mixing rate decreases.[1,2] A means of enhancing this mixing to increase the efficiency would be advantageous. This work is part of a fundamental study of the mixing process in supersonic shear layers with the goal of developing the understanding necessary to develop more efficient mixing processes.

Extensive experiments on subsonic shear layers[3–5] have demonstrated conclusively the importance of developing an understanding of the large-scale turbulence structure before a more complete understanding of the mixing processes can be reached. Until recently, conclusive evidence regarding the structure of the large-scale instabilities in high-speed shear layers had been lacking. There are numerous reports presenting flow visualization of two-dimensional Kelvin–Helmholtz-like structures at moderate convective Mach numbers, up to about 0.6.[2,6,7] However, above this convective Mach number, the visualizations lose clarity, and three dimensionality is assumed to play an important role. There are few direct measurements of the structures because of the difficulty of measuring this type of flowfield, and the difficulty of statistical data analysis associated with the typical high-frequency content related to high-speed flows. Gropengieser,[8] Tam and Hu,[9] and Morris et al.[10] have all used a quasilinear stability analysis to predict that as the convective Mach number increases, the dominant instability waves switch from two- to three-dimensional structures. The predominantly circumstantial evidence from experiments corroborates these predictions.

A unique aspect of the present work is that it focuses on a shear-layer flow in a reduced Reynolds number environment. The reduced Reynolds number is produced by operating with the test-section static pressure well below atmospheric pressure. This approach provides numerous advantages. First, the reduced Reynolds number results in a suppression of the small-scale turbulence, due to viscous forces. This focuses attention on the remaining large-scale turbulent structures, or instability waves. These instabilities are very concentrated in frequency and coherent over somewhat long streamwise distances. Also, these instabilities represent a good characterization of the shear-layer turbulence structures. The second advantage of the reduced Reynolds number is that glow discharge excitation can be used to introduce a perturbation at a chosen frequency in the shear layer. This technique only works at low pressures and densities. Finally, with the low-density conditions and corresponding low dynamic pressure, standard hot-wire probes can be used with fewer wire-breakage problems.

The main disadvantage of this low-to moderate-Reynolds-number facility is that experiments cannot be performed in the high-Reynolds-number environment typically encountered in physical applications. However, in the current work, the large-scale structures are investigated and there is evidence that they are Reynolds-number independent. In low-speed shear layers, Roshko[11] showed that increasing the Reynolds number does not affect the Kelvin–Helmholtz instabilities but increases the smaller-scale turbulence. On the basis of the similarities in the large-scale structures between the incompressible and compressible mixing layers, we conjecture that the Reynolds number will not influence the measured characteristics of

Presented as Paper 94-0822 at the AIAA 32nd Aerospace Sciences Meeting, Reno, NV, Jan. 10–13, 1994; received Jan. 12, 1995; revision received Nov. 13, 1995; accepted for publication Nov. 18, 1995.

*Research Assistant, Department of Aerospace Engineering; currently Postdoctoral Fellow, Aeronautical and Astronautical Research Laboratory, Department of Mechanical Engineering, Ohio State University, 2300 West Case Road, Columbus, OH 43235. Member AIAA.

†Research Assistant, Department of Aerospace Engineering; currently Engineer, General Electric Aircraft Engines, 1 Neumann Way, Mail Drop T34, Cincinnati, OH 45215. Member AIAA.

‡Professor and Head of Aerospace Engineering. Associate Fellow AIAA.

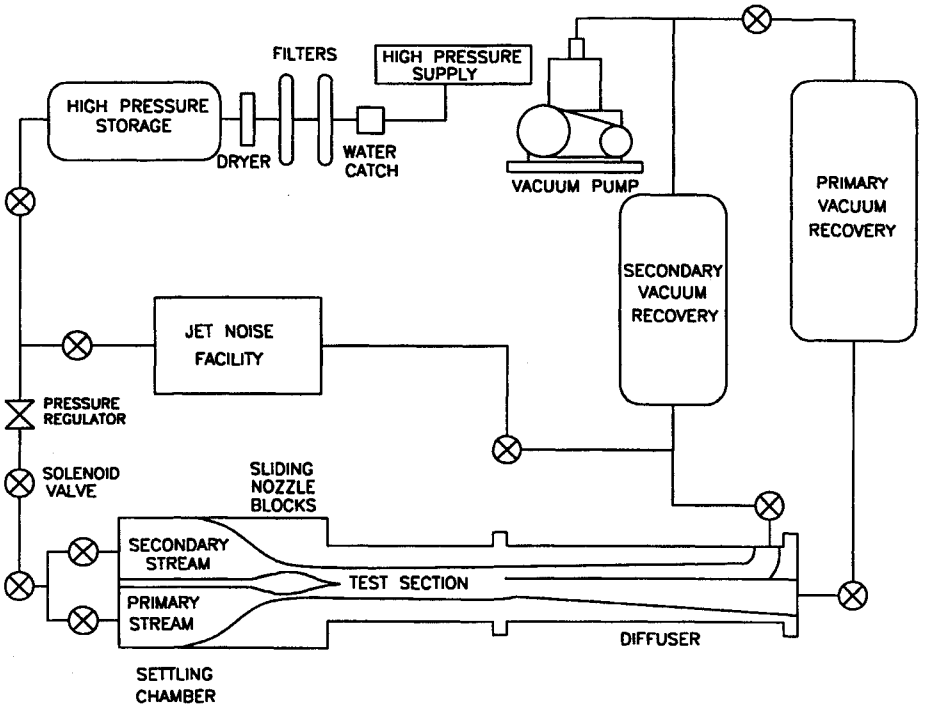

Fig. 1 Schematic of supersonic-shear-layer facility.

the large-scale turbulence structures and/or instability waves to any significant extent.

Martens et al.[12] presented a body of work employing artificial excitation to measure both two- and three-dimensional large-scale structures in supersonic shear layers. Using a glow-discharge technique, instability waves at a specified frequency were excited. From schlieren observations and hot-wire fluctuation spectra, it was clear that this resulted in a dominant instability at the excitation frequency. Methods were developed to measure the basic wave properties of the dominant spectral components, including the wavelengths and the propagation direction of the instability waves. To our knowledge, this was the first work to conclusively show the existence of three-dimensional structures through quantitative measurement techniques. The conclusions from this work were that for a theoretical convective Mach number of 0.5, two-dimensional excitation results in two-dimensional instability waves. Three-dimensional waves were measured when the shear layer, with a theoretical convective Mach number of 0.64, was excited at an oblique angle. When the same shear layer was excited two dimensionally the results were inconclusive. Limitations of these measurements arose from the relatively large spacing in the spanwise direction of the two hot wires used in the experiments. This spacing resulted in a large uncertainty in resolving the spanwise wavelength.

As with the earlier work,[12] the main objective of this work continues to be to provide conclusive experimental evidence to corroborate the aforementioned analytical and/or numerical predictions regarding the nature of the instabilities in high-speed shear layers. The present work is an extension of Martens et al.[12] using upgraded measurement systems and data analysis techniques. This combination increases the accuracy of measurements and clarifies the initial results presented by Martens et al.[12] Extensive measurements performed with four hot wires located at the same axial and vertical position in the shear layer, spaced across the shear layer in the spanwise direction, are presented in this study. Two- and three-dimensional excitation is used to acquire phase distributions, from hot-wire measurements. These distributions are analyzed to determine the angle at which the instability waves convect. This work also serves as a knowledge base for future work in characterizing the instability waves, which are vital to mixing in supersonic shear layers.

Facility

Figure 1 is a schematic of the supersonic-shear-layer facility and accompanying supersonic jet noise facility at Pennsylvania State

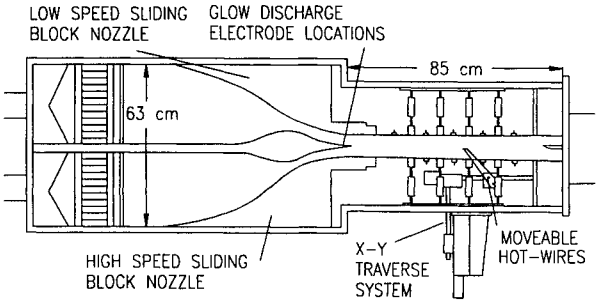

Fig. 2 Schematic of supersonic-shear-layer facility test section.

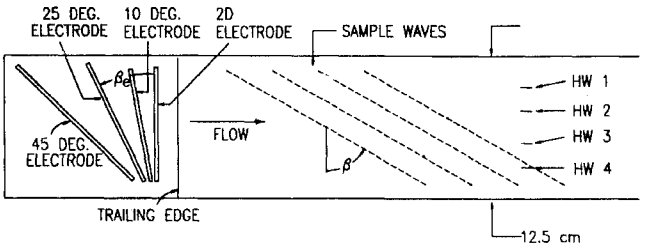

Fig. 3 Schematic of electrodes and hot-wire probes.

University, discussed extensively by Martens et al.[12] and Martens.[13] A schematic of the test section is shown in Fig. 2. Two stacked, sliding block nozzles and a contoured centerbody produce uniform, adjacent supersonic streams. The flow passage is 5.5 cm high, 12.5 cm wide, and 75 cm long. Separate valves allow control of the stagnation pressures and matching of the static pressures at the exit of the nozzles.

Static-pressure taps are mounted flush on the top and bottom walls along the length of the test section. A two-dimensional probe drive penetrates the bottom wall of the test section and can hold either four hot-wire probes or a 5-hole pitot probe rake. Hot-wire anemometers are used extensively to perform a variety of measurements. In this paper, phase-averaged instantaneous hot-wire signals, hot-wire fluctuation spectra, and the phase differences between spectral components of the hot-wire signals are presented. Four hot wires are attached to the probe drive so that they are at the same vertical and axial position in the shear layer and can be traversed both vertically and axially, as a single unit. Figure 3 shows the positions of the four

hot wires. The spacings between probes 1 and 2, 1 and 3, and 1 and 4 are 2.1, 4.96, and 7.06 cm, respectively. The pitot rake can be used to produce both Mach number and velocity profiles.

The glow-discharge excitation system used in these experiments consists of four strip electrodes, also shown in Fig. 3. One is normal to the flow ($\beta_e = 0$ deg), to excite the two-dimensional instabilities, and three are oblique electrodes ($\beta_e = 10$, 25, and 45 deg), to excite three-dimensional instability waves. Only one oblique electrode is in place at a time. The electrodes are made of 0.05-mm-thick copper tape and are 2.0 mm wide. The two-dimensional and 10-deg electrodes are 10 cm long, the 25-deg electrode is 10.5 cm long, and the 45-deg electrode is 14 cm long. The electrodes are attached to, but insulated from, the low-speed side of the aluminum centerbody, near the trailing edge. A 350-V oscillating signal, offset by −400 V DC, is passed through the electrode, producing a glow between the copper and the aluminum, when a threshold voltage is reached. Locally, a very high temperature, this glow produces a disturbance that slightly perturbs the flow adjacent to the electrode.

Since the oblique electrodes travel upstream along the centerbody, there is a velocity differential along the length of the electrode. As a result, the disturbance skews from its original orientation as it convects off the centerbody. This causes the effective excitation angle to be significantly higher than the physical angle of the electrode. There is no velocity differential across the $\beta_e = 0$ and 10-deg electrodes as they are attached to the centerbody in a constant-velocity region. The electrode attached at $\beta_e = 25$ deg warps to an angle of $\beta = 35$ deg, for the Mach 3 case, and $\beta = 44$ deg for the Mach 4 case. Similarly, the $\beta_e = 45$ deg electrode warps to $\beta = 57$ deg for the Mach 3 case, and $\beta = 64$ deg for the Mach 4 case. These angles are all approximate because the velocity is continuously changing in the region between the leading and trailing edges of the electrodes.

Experimental Conditions

All of the experiments reported in this paper were performed at two Mach-number conditions, listed in Table 1. The theoretical convective Mach number is calculated using the equation given by Papamoschou[14]: $M_{c(\text{theor})} = (U_1 - U_2)/(a_1 + a_2)$. The Reynolds numbers reported in Table 1 are based on the conditions in the high-speed stream. Condition I ($M_1 = 3$), at $Re = 40{,}000$/cm transitions from laminar to turbulent flow at approximately 20 cm downstream of the trailing edge. The experiments discussed in the following sections range from 8 to 33 cm downstream. In the case of condition II ($M_1 = 4$), the same Reynolds number (40,000/cm) results in a laminar-to-turbulent transitional shear layer throughout the extent of the measurement locations. It has been shown in low-speed shear layers that the large-scale structures of interest are present in both initially laminar and turbulent shear layers, and are not strongly Reynolds-number dependent.[15]

Mach-Number Profiles

The first experiments discussed are time-averaged measurements using a five-hole pitot probe rake. The measured pitot and static pressures at the same axial location are used in the Rayleigh–pitot formula to calculate the Mach number. The rake is incrementally traversed across the shear layer in a series of experimental runs to produce the Mach-number profiles seen in Figs. 4 and 5, conditions I and II, respectively. Each figure shows the natural and the excited

Table 1 Experimental conditions

Condition	I	II
M_1	3	4
M_2	1.2	1.2
$M_{c(\text{theor})}$	0.5	0.64
a_1, m/s	206	167
a_2, m/s	303	301
U_1, m/s	618	668
U_2, m/s	364	361
P_{01}, kPa	43	103
Re, cm^{-1}	40,000	40,000
Excitation frequency, f_e kHz	25	20

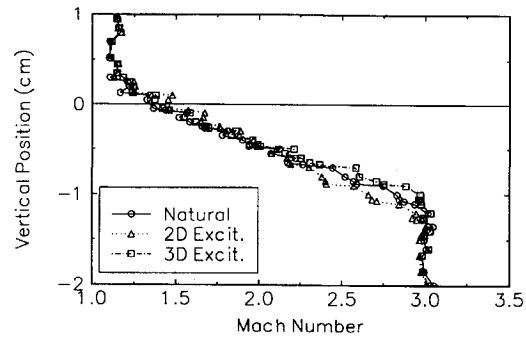

Fig. 4 Mach-number profiles, condition I ($M_1 = 3$), 26 cm downstream.

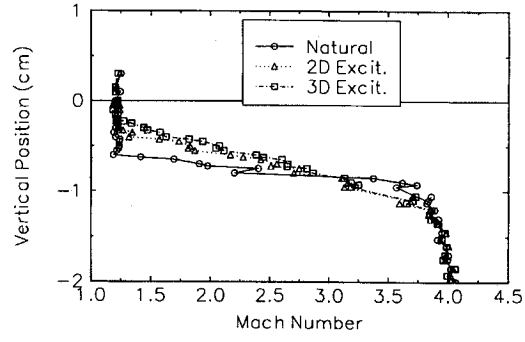

Fig. 5 Mach number profiles, condition II ($M_1 = 4$), 26 cm downstream.

shear layer: in the $M_1 = 3$ case (Fig. 4), a two-dimensional electrode is used; and in the $M_1 = 4$ case (Fig. 5) a 45-deg oblique electrode is used. Figure 4 shows the Mach-number profile across the shear layer, corresponding to condition I ($M_1 = 3$), 26 cm downstream. There is very little effect of excitation at these conditions; the size and shape of the shear layer are virtually unchanged. However, for condition II ($M_1 = 4$) shown in Fig. 5, at the same downstream location, there is a significant increase in the thickness of the shear layer with excitation. This shows that artificial excitation can greatly influence the mean properties of the shear layer, under transitional conditions. Alone, this result indicates an increased growth rate for the $M_1 = 4$ excited shear layer. However, as shown by Martens,[13] both experimental conditions show a thicker shear layer in the transitional region but upon reaching fully turbulent conditions the thickness growth rates of the excited shear layers return to those of the natural cases.

Hot-Wire Fluctuation Spectra

Four hot-wire probes are used simultaneously in these experiments. These four signals are acquired along with the signal triggering the glow-discharge excitation system, when used. The acquisition rate is 111 kHz and the hot-wire signals are bandpass filtered between 1.5 and 50 kHz. The high-pass filter setting is chosen to cut out any low-frequency facility resonances and the low-pass filter setting is below the Nyquist frequency. Once the data are acquired, they can be analyzed using standard signal-processing techniques. The autospectrum is calculated for each hot-wire signal and, if the experiment involves excitation, the cross spectrum between each hot wire and the glow signal is calculated. The phase difference between two signals (as a function of frequency) is determined as part of the cross spectrum. Figures 6 and 7 show typical hot-wire spectra for the two experimental conditions. Figure 6 is measured for condition I ($M_1 = 3$), 18 cm downstream, and 0.625 cm below the centerline. This is the vertical position of maximum fluctuations, for this axial location. Both the natural case (Fig. 6a) and the two-dimensionally excited case ($f_e = 25$ kHz, Fig. 6b) are shown. The characteristic frequency for Fig. 6a is 41 and 43 kHz for Fig. 6b. Figure 7 shows the results for condition II ($M_1 = 4$), 27 cm downstream, and 0.875 cm below the centerline, again at the position of maximum fluctuations. Similarly, Fig. 7a corresponds to the natural shear layer, $f_c = 85$ kHz, and Fig. 7b corresponds to the three-dimensionally

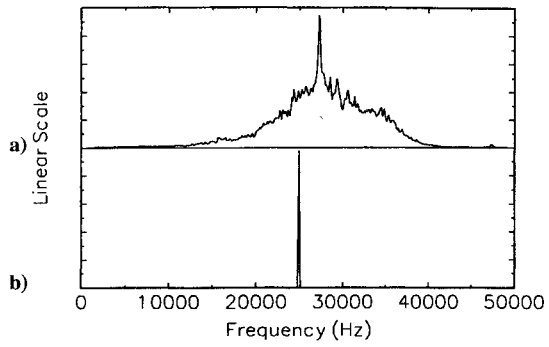

Fig. 6 Hot-wire power spectra, condition I (M_1 = 3), 18 cm downstream, 0.625 cm below the centerline: a) natural, f_c = 41 kHz and b) two dimensional, f_e = 25 kHz, f_c = 43 kHz.

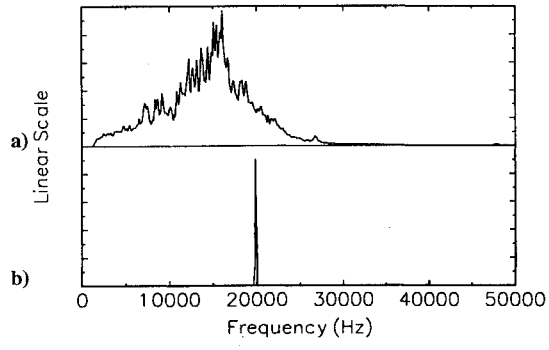

Fig. 7 Hot-wire power spectra, condition II (M_1 = 4), 27 cm downstream, 0.875 cm below the centerline: a) natural, f_c = 85 kHz and b) 25 deg electrode, f_e = 20 kHz, f_c = 46 kHz.

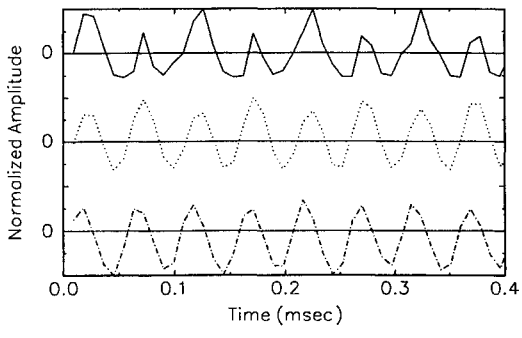

Fig. 8 Phase-averaged signals, condition II (M_1 = 4), 27 cm downstream, 0.875 cm below the centerline, 25-deg electrode, f_e = 20 kHz. The sampling time interval is 9 μs: ——, excitation signal; ....., hot-wire 3; and –.–.–.–, hot-wire 4.

(β_e = 25 deg) excited case (f_e = 20 kHz), f_c = 46 kHz. In the latter case, the characteristic frequency is greatly reduced because the shear-layer thickness has approximately doubled because of the excitation.

The spectra measured in the present moderate-Reynolds-number experiments are similarly shaped, but not quite as broad in frequency as those measured in more conventional high-Reynolds-number shear layers by Shau et al.[16] In the present experiments, the excitation frequency is typically chosen as the frequency corresponding to the highest level on a fluctuation spectrum measured in the upstream sections of the test section.[13] In Figs. 6b and 7b, the effect of the glow-discharge excitation is seen. Virtually all of the energy in the flow becomes concentrated in a narrow frequency band around the excitation frequency. As seen in Figs. 6b and 7b, the hot-wire spectra for the two- and three-dimensionally excited shear layers look very similar.

Another important consequence of exciting the flow is that the hot-wire signals can be phase averaged. Figures 6b and 7b show that there is only one frequency component present, and this should

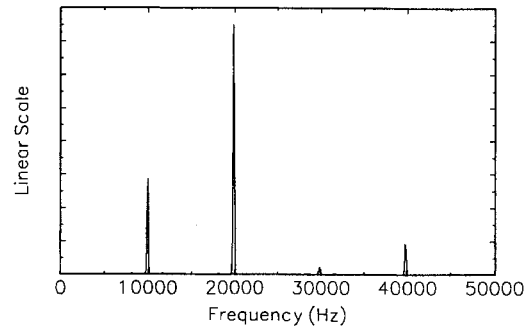

Fig. 9 Cross spectrum between the excitation signal and hot-wire 1, condition II (M_1 = 4), 27 cm downstream, 0.875 cm below the centerline, f_e = 20 kHz, 25-deg electrode.

clearly show up in the time signal as a harmonic wave. Figure 8 shows the phase-averaged portions of the excitation signal and two of the hot-wire signals, formed from data acquired at the same axial position as Fig. 7b. These phase-averaged signals are constructed by using the excitation signal as a reference and averaging the hot-wire signals over many periods.

A new feature of the experimental procedure is that the amplitude of the excitation frequency is modulated by mixing two signals, one at the desired excitation frequency, f_e, and the other at half that frequency, $f_e/2$. The magnitude of the subharmonic component is approximately 40% that of the fundamental component. The amplitude modulation is not as pronounced in the hot-wire signals, but it is present. This method helps determine if two hot wires are measuring the same oblique wave, or if there is a complete wavelength or more between the two hot wires so that they are measuring different waves. Although excitation at $f_e/2$ is not easily visible in the excited spectra, because of the linear scale (Figs. 6b and 7b), it is prominent in the associated cross spectrum between the excitation signal and the hot-wire signal. Figure 9 shows the cross spectrum for the conditions of Fig. 7b. The magnitude of the 10-kHz peak is less than half that of the 20-kHz peak.

Results of Phase Measurements

When the shear layer is excited using glow-discharge excitation, two important functions are achieved. First, as seen previously, the hot-wire fluctuation spectra collapse to the chosen excitation frequency, and, second, the signal used to trigger the electrode can be used as a phase reference. One goal of these experiments is to determine the orientation of the instability waves in the shear layer. To determine this, both the wavelength in the axial direction and the wavelength in the spanwise direction are needed. To find these wavelengths, the phase as a function of axial and spanwise distance must be found. There is a large amount of data amassed in these experiments, and so, for brevity, one condition is chosen and the methodology is outlined in detail. A summary is then presented for other cases.

Condition II (M_1 = 4) is discussed here, excited with the β_e = 25-deg electrode. This case is chosen because it is one of the more complicated cases, resulting in oblique instability waves. Figure 10 shows the phase between each hot wire and the excitation signal, as a function of downstream distance. As reported previously,[12] the wavelength is constant throughout the length of the test section. On this figure, the data from each of the four hot wires are shown, resulting in four approximately parallel lines. Then, the axial wavelength λ is found by the simple relation $\lambda = 360$ deg/m, where m is the slope of one of the lines in Fig. 10. The resulting wavelength from the graph is 3.2 cm. Table 2 shows the measured axial wavelength for each experimental case. It is seen that there is very little change for each excitation case at a given experimental condition. The variations in the measured wavelengths for condition I are attributed to slightly different velocity and frequency settings between experiments as well as experimental uncertainty. Another factor influencing these measurements is the effect of the side walls on these large-scale structures. The portions near the sides may be skewed because of interactions with the walls. Deformations due to the side walls are

Table 2 Axial wavelengths

Experimental condition	Excitation frequency f_e, kHz	Excitation angle β_e, deg	Axial wavelength, cm
I	25	0	1.9
I	25	25	2.4
I	25	45	1.8
II	20	0	3.2
II	20	10	3.2
II	20	25	3.2
II	20	45	3.2

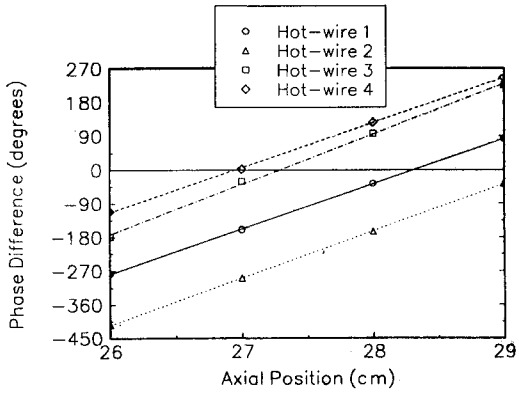

Fig. 10 Phase difference between the 20-kHz component of the hot wire and excitation signals as a function of downstream distance, condition II (M_1 = 4), excited with the 25-deg electrode.

seen in the far wake visualizations of Williamson and Prasad.[17,18] The values for the two-dimensionally excited cases have been verified through schlieren photographs of the two-dimensionally excited shear layer, where the large-scale structures appear very clearly.[12] With the excitation signal constructed from sine waves at f_e and $f_e/2$, the wavelength can be calculated from both portions of the signal. The measured corresponding wavelength for the conditions of Fig. 10 for the 10-kHz portion of the signal is 6.4 cm. This shows that the axial convection velocity—axial wavelength multiplied by the frequency ($U_c = \lambda * f$)—is the same for both frequency modes. This agrees with the computations of Gathmann et al.[19] who show that different Kelvin–Helmholtz modes travel with the same velocity. This method helps check the accuracy of these measurements, since the wavelength for the 10-kHz portion should always be twice the wavelength of the 20-kHz signal, that is, if the frequency is halved, the wavelength will be doubled. The convection velocity is approximately 508 m/s for condition I (M_1 = 3) and 640 m/s for condition II (M_1 = 4). These convection velocities result in convective Mach numbers of $M_{c1} = 0.51$ and $M_{c2} = 0.49$ for condition I ($M_{c(\text{theor})} = 0.5$) and $M_{c1} = 0.19$ and $M_{c2} = 0.9$ for condition II ($M_{c(\text{theor})} = 0.64$).

Determining the spanwise wavelength is more difficult. Because of the limited number of the spanwise measurement locations (and their spacing), it is difficult to determine whether all or some of the hot wires are measuring points on the same wave. If the spanwise wavelength is less than the separation distance between two hot wires, they will measure points on different waves. (As the propagation angle of the structure increases, the spanwise wavelength decreases.) If this occurs, then the values of phase difference between two hot wires will be off by $n * 360$ deg, where n is the number of waves between the two hot wires. Because both frequencies in the excitation signal have been shown to result in the same convection velocity, both may be used to calculate the wave propagation angles, which should be identical.

The first step in determining the spanwise wavelength is making a profile of the phase between each hot wire and the excitation signal. This is shown in Fig. 11 for condition II (M_1 = 4), 27 cm downstream. The phase-averaged hot-wire signals are used to determine if the hot wires are measuring the same wave or are measuring points on different waves (predominantly by examining the subharmonic

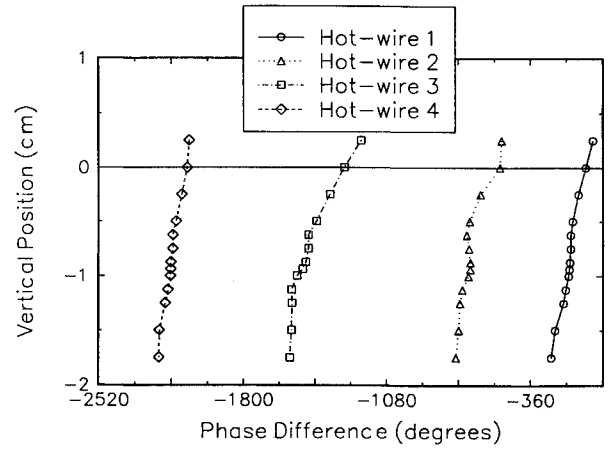

Fig. 11 Phase profiles between the 20-kHz component of the hot wire and the excitation signal, condition II (M_1 = 4), 27 cm downstream, excited with the 25-deg electrode.

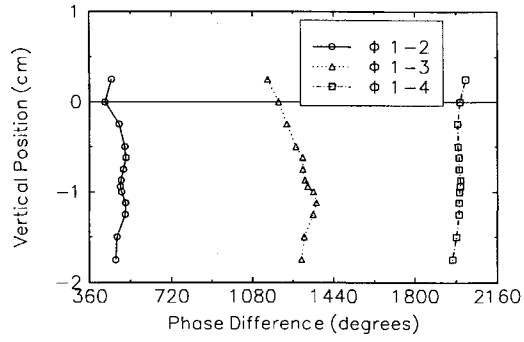

Fig. 12 Phase profiles between the 20-kHz component of the signal from hot-wire 1 and the other hot-wire signals, condition II (M_1 = 4), 27 cm downstream, excited with the 25-deg electrode.

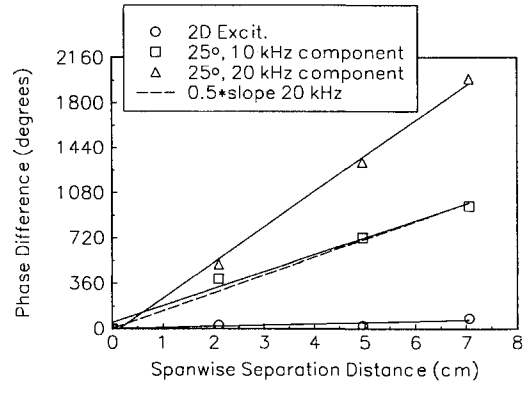

Fig. 13 Spanwise separation between hot-wire signals vs phase difference between hot wires, condition II (M_1 = 4), 27 cm downstream, excited with the 25-deg electrode.

wave). The appropriate integer multiple of 360 deg is then added or subtracted from the phase.

Next, the phase difference between each hot wire with respect to hot-wire 1 is found. This is shown in Fig. 12 for the same conditions. In this figure, it is seen that there is a region of fairly constant phase difference from 0.8 to 1.0 cm below the centerline. This linear region coincides with the location of the maximum fluctuation levels in the shear layer. The phase difference in this region is plotted against the spanwise separation distance of the hot wires, shown in Fig. 13. The slopes of the lines on this graph result in the spanwise wavelength, 360 deg/m. The resulting spanwise wavelengths are 2.7 cm for the 10-kHz signal and 1.3 cm for the 20-kHz signal, for condition II (M_1 = 4). The dotted line corresponds to one-half the slope of the 20-kHz line. Taken with the previously determined

Table 3 Spanwise wavelengths and propagation angles

Experimental condition	Excitation frequency f_e, kHz	Excitation electrode, deg	Actual excitation angle, deg	Axial measurement location, cm	Spanwise wavelength, cm	Propagation angle, deg
I	25	0	0	8, 18, 23, 33	15, 32, 49, 59	7, 3, 2, 2
I	25	25	35	27	1.5	58
I	25	45	57	8, 18, 23, 33	1.3, 1.3, 1.4, 1.6	54, 55, 52, 48
II	20	0	0	10, 27	57, 36	3, 5
II	20	10	10	10, 26	1.27, 1.35	63, 64
II	20	25	44	10, 27	1.3, 1.3	66, 68
II	20	45	64	27	1.6	61

axial wavelengths, the wave angles can be calculated as 67 deg for the 10-kHz signal and 68 deg for the 20-kHz signal. Figure 3 shows the defined propagation angle β of the large-scale structures ($\beta = 0$ deg corresponds to a two-dimensional structure). Also shown in Fig. 13 are the results for the same experimental conditions but with two-dimensional excitation. If these instability waves were perfectly two-dimensional, the line would be horizontal at zero phase difference. The slight slope present is attributed to either experimental uncertainty or a slight warping of the two-dimensional structure near the side walls of the test section. For all experimental conditions, the two-dimensional excitation results in virtually two-dimensional instability waves. Table 3 lists the spanwise wavelength and resulting wave angle for all cases investigated. The experimental uncertainty in the wave-angle measurement is estimated to be ± 7 deg.

For both experimental conditions when the shear layer is excited with the two-dimensional electrode, the instability waves remain two-dimensional (± 7 deg) throughout the test section. From the results listed in Table 3 the conclusion reached is that for condition I ($M_1 = 3$) an oblique instability wave traveling at 53 ± 7 deg results when the shear layer is excited with electrodes at angles of 25 or 45 deg. Similarly, for condition II ($M_1 = 4$), 10-, 25-, and 45-deg excitation results in an oblique instability wave traveling at 64 ± 7 deg. This points to the conclusion that the shear layer naturally contains a preferred oblique angle for instability wave propagation, and regardless of the oblique excitation angle, the instability waves tend toward the preferred angle. The trend of higher propagation angles with higher velocities also agrees with theoretical predictions.[8–10] For some experimental conditions, these measurements were repeated at several axial locations and resulted in similar propagation angles, also listed in Table 3. Sandham and Reynolds[20] presented an equation relating the propagation angle to the convective Mach number, for $M_{c(\text{theor})}$ above 0.6: $M_{c(\text{theor})} \cos(90 - \beta) \approx 0.6$. Solving for the propagation angle for condition II, $M_{c(\text{theor})} = 0.64$, results in $\beta = 69.6$ deg, well within the uncertainty range of the present work. Also, calculating the wave angles for both the f_e and $f_e/2$ excitation resulted in virtually identical wave angles, within the experimental uncertainty. The computational results of Gathmann et al.[19] and visualizations of Samimy et al.[21] show Λ-shaped structures formed by two oblique Kelvin–Helmholtz instability wave pairs. In particular, the computations of Gathmann et al.[19] show the same type of phase dislocations in the spanwise direction as determined in the low-speed mixing-layer experiments of Browand and Troutt.[15] In the present experiments, a single oblique mode is excited. However, there may be additional waves traveling in the opposite oblique direction that cause similar phase dislocations that contribute to the experimental uncertainty. Visualizations of the far-wake structure downstream of a cylinder by Williamson and Parsad[17,18] show oblique structures propagating predominantly in one direction with some evidence of a crisscross pattern (pairs of oblique waves at equal but opposite angles).

Conclusions and Future Work

Mach-number profiles have been measured for two Mach-number conditions. Artificial excitation was used and, for the higher Mach-number case, a significantly thicker Mach-number profile was observed compared to the natural case. Four hot wires were used simultaneously to measure the characteristics of the instability waves present in the supersonic shear layer. Excitation was applied to either two- or three-dimensional waves and to provide a consistent phase reference. In both Mach-number cases, two-dimensional excitation resulted in instability waves that remained virtually two-dimensional throughout the test section. This clarifies the results of Martens et al.,[12] which did not determine the orientation of the instability waves for condition II ($M_1 = 4$) with two-dimensional excitation. Three-dimensional excitation resulted in oblique instability waves. For different excitation angles, a similar resulting oblique wave angle developed in each experimental condition. Also, as expected, the higher Mach-number case resulted in a higher propagation angle.

This is a major step in accurately measuring oblique instability waves in the supersonic shear layer. The methodology and technology have been proven and may now be applied to more complicated geometries and conditions. It is anticipated that in the near future, wavy walls will be installed and tested as a mixing-enhancement method. The idea is to create a system of Mach waves with the wavy wall that interact with the acoustic waves or the Kelvin–Helmholtz instability waves in such a way as to increase the growth rate, as discussed by Tam and Hu.[22] The methods presented herein will be required to investigate that more complicated situation.

Acknowledgments

This research project was supported by NASA Lewis Research Center through Grant NAG-3-1492, with Technical Officers K. B. M. Q. Zaman and R. R. Mankbadi. The authors thank I. M. Blankson of NASA Headquarters for his continuing support and P. J. Morris for his helpful suggestions.

References

[1]Bogdanoff, D. W., "Compressibility Effects in Turbulent Shear Layers," *AIAA Journal*, Vol. 21, No. 6, 1983, pp. 926–927.

[2]Papamoschou, D., and Roshko, A., "The Compressible Turbulent Shear Layer: An Experimental Study," *Journal of Fluid Mechanics*, Vol. 197, Dec. 1988, pp. 453–477.

[3]Winant, C. D., and Browand, F. K., "Vortex Pairing: The Mechanism of Turbulent Mixing at Moderate Reynolds Numbers," *Journal of Fluid Mechanics*, Vol. 63, Pt. 2, 1974, pp. 237–255.

[4]Huang, L. S., and Ho, C. M., "Small-Scale Transition in a Plane Mixing Layer," *Journal of Fluid Mechanics*, Vol. 210, 1990, pp. 475–500.

[5]Oster, D., and Wygnanski, I., "The Forced Mixing Layer Between Parallel Streams," *Journal of Fluid Mechanics*, Vol. 123, pp. 91–130.

[6]Hall, J. L., Dimotakis, P. E., and Rosemann, H., "Experiments in Non-Reacting Compressible Shear Layers," AIAA Paper 91-0629, Jan. 1991.

[7]Clemens, N. T., and Mungal, M. G., "Two- and Three-Dimensional Effects in the Supersonic Mixing Layer," *AIAA Journal*, Vol. 30, No. 4, 1992, pp. 973–981.

[8]Gropengieser, H., "Study on the Stability of Boundary Layers and Compressible Fluids," NASA TT F-12, 786, May 1969.

[9]Tam, C. K. W., and Hu, F. Q., "The Instability and Acoustic Wave Modes of Supersonic Mixing Layers Inside a Rectangular Duct," *Journal of Fluid Mechanics*, Vol. 203, 1989, pp. 51–76.

[10]Morris, P. J., Giridharan, M. G., and Viswanathan, K., "Turbulent Mixing in Plane and Axisymmetric Shear Layers," AIAA Paper 90-0708, Jan. 1990.

[11]Roshko, A., "Structures of Turbulent Shear Flows: A New Look," *AIAA Journal*, Vol. 14, No. 10, 1976, pp. 1349–1357.

[12]Martens, S., Kinzie, K. W., and McLaughlin, D. K., "Measurements of Kelvin–Helmholtz Instabilities in a Supersonic Shear Layer," *AIAA Journal*, Vol. 32, No. 8, 1994, pp. 1633–1639.

[13]Martens, S., "An Experimental Study of Compressible Mixing Layers," Ph.D. Thesis, Dept. of Aerospace Engineering, Pennsylvania State Univ., University Park, PA, 1995.

[14]Papamoschou, D., "Structure of the Compressible Turbulent Shear Layer," AIAA Paper 89-0126, Jan. 1989.
[15]Browand, F. K., and Troutt, T. R., "The Turbulent Mixing Layer: Geometry of Large Vortices," *Journal of Fluid Mechanics*, Vol. 158, No. 7, 1985, pp. 489–509.
[16]Shau, T. R., Dolling, D. S., and Choi, K. Y., "Organized Structure in a Compressible Turbulent Shear Layer," *AIAA Journal*, Vol. 31, No. 8, 1993, pp. 1398–1405.
[17]Williamson, C. H. K., and Prasad, A., "A New Mechanism for Oblique Wave Resonance in the 'Natural' Far Wake," *Journal of Fluid Mechanics*, Vol. 256, 1993, pp. 269–313.
[18]Williamson, C. H. K., and Prasad, A., "Acoustic Forcing of Oblique Wave Resonance in the Far Wake," *Journal of Fluid Mechanics*, Vol. 256, 1993, pp. 315–341.
[19]Gathmann, R. J., Si-Ameur, M., and Mathey, F., "Numerical Simulations of Three-Dimensional Natural Transition in the Compressible Confined Shear Layer," *Physics of Fluids*, Vol. 5, No. 11, 1993, pp. 2946–2968.
[20]Sandham, N. D., and Reynolds, W. C., "Compressible Mixing Layer: Linear Theory and Direct Simulation," *AIAA Journal*, Vol. 28, No. 4, 1990, pp. 618–624.
[21]Samimy, M., Reeder, M. F., and Elliott, G. S., "Compressibility Effects on Large Structures in Free Shear Flows," *Physics of Fluids*, Vol. 4, No. 6, 1992, pp. 1251–1258.
[22]Tam, C. K. W., and Hu, F. Q., "Resonant Instability of Ducted Free Supersonic Mixing Layers Induced by Periodic Mach Waves," *Journal of Fluid Mechanics*, Vol. 229, 1991, pp. 65–85.